Preferential particle concentration in wall-bounded turbulence with zero skin friction

Kun Yang, Lihao Zhao, and Helge I. Andersson

Citation: Physics of Fluids **29**, 113302 (2017);
View online: https://doi.org/10.1063/1.4998547
View Table of Contents: http://aip.scitation.org/toc/phf/29/11
Published by the American Institute of Physics

Preferential particle concentration in wall-bounded turbulence with zero skin friction

Kun Yang,[1] Lihao Zhao,[1,2,a)] and Helge I. Andersson[1]
[1]*Department of Energy and Process Engineering, Norwegian University of Science and Technology, 7491 Trondheim, Norway*
[2]*Department of Engineering Mechanics, Tsinghua University, 10084 Beijing, China*

(Received 1 August 2017; accepted 21 October 2017; published online 16 November 2017)

Inertial particles dispersed in turbulence distribute themselves unevenly. Besides their tendency to segregate near walls, they also concentrate preferentially in wall-parallel planes. We explore the latter phenomenon in a tailor-made flow with the view to examine the homogeneity and anisotropy of particle clustering in the absence of mean shear as compared with conventional, i.e., sheared, wall turbulence. Inertial particles with some different Stokes numbers are suspended in a turbulent Couette-Poiseuille flow, in which one of the walls moves such that the shear rate vanishes at that wall. The anisotropies of the velocity and vorticity fluctuations are therefore qualitatively different from those at the opposite non-moving wall, along which quasi-coherent streaky structures prevail, similarly as in turbulent pipe and channel flows. Preferential particle concentration is observed near both walls. The inhomogeneity of the concentration is caused by the strain-vorticity selection mechanism, whereas the anisotropy originates from coherent flow structures. In order to analyse anisotropic clustering, a two-dimensional Shannon entropy method is developed. Streaky particle structures are observed near the stationary wall where the flow field resembles typical wall-turbulence, whereas particle clusters near the moving friction-free wall are similar to randomly oriented clusters in homogeneous isotropic turbulence, albeit with a modest streamwise inclination. In the absence of mean-shear and near-wall streaks, the observed anisotropy is ascribed to the imprint of large-scale flow structures which reside in the bulk flow and are global in nature. *Published by AIP Publishing.* https://doi.org/10.1063/1.4998547

I. INTRODUCTION

Turbulent particle suspension flow is a topic of great relevance in several natural and industrial applications and has therefore been studied extensively over many decades. Due to the complex nature of turbulence, particle motion is to a great extent random. Inertial particles suspended in a fluid are transported by the flow, and their inertia determines how the particles follow the flow. Particle inertia is often measured by the non-dimensional Stokes number, defined as the ratio of a particle time scale to a fluid time scale. An interesting phenomenon of inertial spherical particles in turbulence is the inhomogeneity of the particle distribution,[1] often referred to as particle preferential concentration, i.e., inertial particles preferentially cluster in certain regions of the flow and form voids in other regions.

In the literature, discussions of particle preferential concentration have been mostly devoted to homogeneous isotropic turbulence (HIT), for which it is observed that particles tend to accumulate in regions of high strain and avoid regions of high vorticity, thereby forming filaments and voids.[2,3] This mechanism can be referred to as strain-vorticity-selection and is attributed to the centrifugal effect of the local fluid eddies. In HIT, the particle Stokes number is defined by the Kolmogorov time scale, τ_K, i.e., $St_K = \tau_p/\tau_K$, and the particles will demonstrate the strongest clustering when the particle response time τ_p matches the fluid time scale,[4] i.e., $St_K \approx 1$. However, it is noted by Monchaux *et al.*[1] that the explanation of centrifugal effects on particle clustering fails for moderately high St_K. Another mechanism to explain preferential clustering is the so-called sweep-stick mechanism,[5] which causes the inertial particles to cluster in regions where the fluid acceleration is perpendicular to the direction of highest contraction between neighbouring particles. Quantification of preferential clustering and characterizing clusters/voids can be challenging, but there are some successful approaches. For a complete review of those methods, the readers are referred to the comprehensive review paper by Monchaux *et al.*[1] One commonly used method for measuring inhomogeneities in particle distributions is the Voronoï diagram,[6] the advantage of which is its independence of a pre-defined grid, as in box counting schemes. For a 3D particle field, the Voronoï volume divides the whole domain into sub-volumes consisting of all points being closer to one particular particle than others and thus provides a specific volume that is the inverse of the local particle number density. This method has been used to quantify particle clustering in both homogeneous flows[4,7,8] and wall-bounded flow.[6,9,10]

Another commonly encountered flow scenario is the wall-bounded flow. Studies on particle dispersion in turbulent channel flows (Poiseuille flows) are mostly focused on wall-normal particle segregation near the walls,[11,12] which is attributed to turbophoresis.[13,14] The segregated particles near the walls also exhibit an inhomogeneous and anisotropic distribution in

a)Electronic mail: zhaolihao@tsinghua.edu.cn

wall-parallel planes.[15–20] Following the near-wall low-speed streaks, the particles in the viscous sublayer also form streamwise streaky patterns and preferentially accumulate in regions of instantaneous streamwise velocity deficit.[2,11,19] Dimensional characteristics such as the spanwise spacing between the streaks can be obtained by the spanwise two-point correlation coefficient of particle concentration fluctuations,[10,20] similar to that used in determining the fluid near-wall low-speed streaks.[21–23] The overall particle wall-normal segregation can be measured by a global Shannon entropy method,[24] which reflects the spatio-temporal evolution of the particle phase (definition given in Sec. II C). The Shannon entropy has been proven to be an effective anisotropy detection method, which has been successfully applied in various three-dimensional distributions, not only for inertial particles in turbulent flows[24–26] but also for cosmological observations.[27]

Other than the quasi-coherent near-wall turbulent structures, many wall-bounded flows form large-scale-structures (LSSs) that occupy almost the whole domain. Examples include turbulent Poiseuille flows (P flows) at high Re_τ[26,28–31] (Re_τ based on the friction velocity u_τ and the channel half-height h) and turbulent Couette flows (C flows) at low or moderate Re_τ.[32–34] In these flows, the non-linear interactions between the coexisting near-wall turbulent streaky structures and the LSSs can be crucial to particle dispersion. However, relevant studies are rare.[20,35,36] In particular, Bernardini *et al.*[20] conducted a direct numerical simulation (DNS) coupled with Lagrangian particle tracking for a turbulent C flow at $Re_\tau = 167$ and compared with a P flow at $Re_\tau = 183$. They considered particles of four different inertia groups and found the highest near-wall segregation at $St = 25$ for both the C flow and the P flow. Particles formed near-wall streamwise streaks in both flows, but the characteristic patterns of the streaks were essentially different between the two flows, as a result of the significant impact from the imprinting of the outer-layer LSSs onto the inner-layer fluid structures. While the C flow is a good choice for evaluating particle distribution under the influences of LSSs, the near-wall structures make it difficult to determine the effects of LSSs separately in the near wall region. In addition, the LSSs formed in a C flow are always quite huge (long streamwise extension), and therefore DNS of C flows usually requires at least 8 times larger computational domain than for P flows to accommodate the LSSs in C flows.[21]

To evaluate the effects of distinct near-wall structures on wall-parallel particle preferential concentration, we investigate a shear-free turbulent Couette-Poiseuille flow (CP flow). By eliminating the mean shear at the moving wall, the quasi-coherent near-wall structures formed only near the stationary wall, leaving effects of the global LSSs alone near the moving wall. The CP flow was used by Thurlow and Klewicki[37] to understand the mechanisms of drag reduction of ultra-hydrophobic surfaces and by Coleman *et al.*[38] to improve turbulence closure models.

One may compare the current CP flow with the turbulent open channel flow, which has a similar asymmetric shear distribution with maximum mean shear at the no-slip wall and zero mean shear at the free-surface.[39,40] However, the two flows are essentially different. First, the wall-normal distributions of the turbulence intensities and the r.m.s. vorticity are distinctly different near the moving wall in the CP flow and the free-slip surface in the open-channel flow, due to the different boundary conditions. Second, the coherent structures (both near-wall and in the bulk of the flow) observed in the two flows are essentially different. The LSSs in an open-channel flow are large-scale upwellings and downwellings across the domain caused by the near-wall sweeps and ejections imprinting from near the no-slip wall to the free-slip surface.[41] On the contrary, in a CP flow, the quasi-coherent near-wall sweep and ejection events are relatively small-scale and confined near the stationary wall, similar to those in a P flow. The LSSs in a CP flow are large-scale longitudinal circulations which are not observed in an open-channel flow at a similar Re_τ.[23,42] Differences in the underlying flow will lead to variations in the corresponding particle preferential concentration near the walls. Particle distributions in open channel flows were studied by van Haarlem *et al.*[16] and Narayanan *et al.*,[17] with the focus on particle wall-normal segregation. However, clustering of inertial particles in the vicinity of a shear-free wall has never been studied before, although it can be anticipated that the presence of a no-slip wall will make the particle concentration pattern qualitatively different from that observed beneath a free surface.

In an accompanying paper,[43] we considered a tailor-made turbulent CP-flow in which the mean shear vanished at the moving wall. We found that inertial particles segregated not only near the stationary wall where mean shear prevailed but also near the moving wall where mean shear was absent. Different physical mechanisms for particle transport in the wall-normal direction were explored and we concluded that the presence of strong quasi-coherent near-wall structures is not a prerequisite for near-wall accumulation of inertial particles. In the present paper, the same five groups of inertial particles are further examined with the view to analyze the anisotropic particle concentration in wall-parallel planes. The current paper is organized as follows: Sec. II presents the numerical methods and also introduces the new 2D Shannon entropy method applied in the study; in Sec. III, the results are presented, whereafter a detailed description of the quantified observations is provided and the underlying mechanisms are evaluated in detail.

II. METHODOLOGY

A. DNS of turbulent CP flow

The carrier flow is a turbulent CP flow with vanishing mean shear at a moving wall, governed by the incompressible Navier-Stokes equation and the continuity equation. The flow configuration is shown in Fig. 1. The flow was solved using DNS, and the relevant parameters are given in Table I. The flow was calculated using an Eulerian approach, with a pseudo-spectral method in the homogeneous (x-, y-) directions, and a second-order central finite-difference method in the wall-normal (z-) direction. The pressure field was obtained by solving a Poisson equation using Fast Fourier Transform (FFT) in the homogeneous directions and a tri-diagonal matrix algorithm in the wall-normal direction. An explicit second-order Adams-Bashforth scheme was used for time

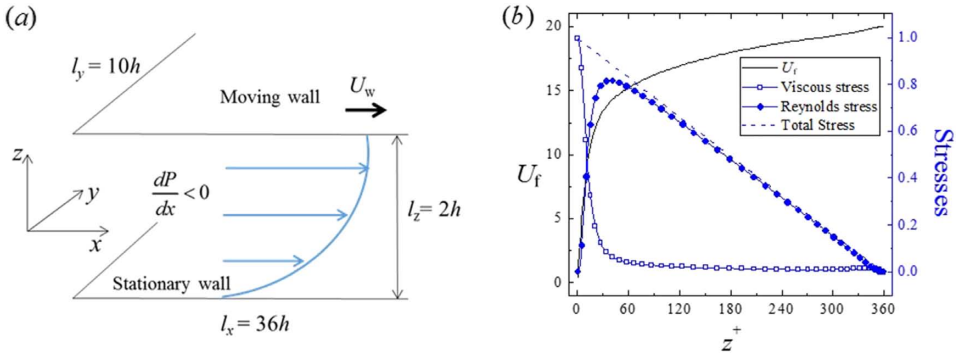

FIG. 1. Properties of the carrying turbulent CP flow. (a) Definition sketch of the CP flow with streamwise-driving pressure and moving wall with velocity U_w. (b) Distribution of the mean streamwise velocity U_f (black line, left vertical axis) and mean shear stresses (blue lines with markers, right vertical axis).

TABLE I. DNS parameters for the turbulent CP flow. The grid size in the homogeneous xy-plane is uniform. In the wall-normal direction, the grid size is non-uniform and symmetric with respect to the channel centre, with the smallest grid spacing $\Delta z^+ = 0.88$ near the walls and the largest grid spacing $\Delta z^+ = 2.86$ in the channel centre. The superscript + denotes normalization using viscous units, $u_{\tau,s}$ for velocity, $\nu/u_{\tau,s}$ for length, and $\nu/u_{\tau,s}^2$ for time, where $u_{\tau,s}$ is the friction velocity at the stationary wall. U_w^+: normalized wall velocity. h: half channel height; l_x, l_y, and l_z: streamwise (x), spanwise (y), and wall-normal (z) length of the computational domain, respectively; N_x, N_y, and N_z: number of grid points in x-, y-, and z-direction, respectively. Δt^+: normalized time step.

$Re_{\tau,s}$	U_w^+	l_x/h	l_y/h	l_z/h	Δx^+	Δy^+	Δz^+	$N_x \times N_y \times N_z$	Δt^+
180	20	36	10	2	11.25	6.93	0.88–2.86	$576 \times 260 \times 192$	0.036

advancement. Negligible mean shear at the moving wall was achieved by properly choosing the wall velocity U_w together with the streamwise-driving pressure gradient. For the present CP flow, we obtained a statistically negligibly low total mean shear of 0.3% as compared with that at the fixed wall [Fig. 1(b)].

Characteristics of the background turbulent CP flow were discussed comprehensively by Yang *et al.*[23,42] The key features relevant to our present discussions are the distinguishing near-wall structures and the co-existing coherent structures of different scales, i.e., the quasi-coherent turbulent structures near the stationary wall and the LSSs which span across the channel. The flow structures near the stationary wall are similar to those in a P flow, where strong turbulent regeneration events occur and streamwise-streaky turbulent structures are formed. These structures are strong but are locally confined only near the stationary wall. In addition, LSSs are observed in the CP flow. They are weak in strength but are global (span across the cross section), with long streamwise correlations and wider spanwise spacing. Since they are global, the LSSs impinge onto the near-wall turbulent structures, causing an increase in their spanwise spacing compared to the conventional P flow case. The interactions between the two scales near the stationary wall were discussed in detail by Yang *et al.*[42]

B. Lagrangian tracking of inertial particles

After the turbulent CP flow had developed into a statistically steady state, inertial particles were added at random locations and tracked at each time step (same as for the Eulerian fluid) in a Lagrangian framework. The current study considers rigid, point-like (i.e., particle size smaller than Kolmogorov microscale) and spherical particles with varying inertia, which are only subjected to a modified Stokes drag force. We consider only a dilute suspension where particle-particle collisions and feedback of particles on the fluid can be neglected. The initial particle velocity was prescribed to equal the local fluid velocity, which was obtained by using a quadratic interpolation scheme applying information from the 27 closest grid-points.[44] The position and velocity of each particle are updated by integration of the following equations forward in time:

$$\frac{d\vec{x}_p}{dt} = \vec{u}_p, \tag{1a}$$

$$\frac{d\vec{u}_p}{dt} = \frac{1}{\tau_p}(\vec{u}_{fp} - \vec{u}_p)(1 + 0.15Re_p^{0.687}), \tag{1b}$$

where $\vec{x}_p = (x_p, y_p, z_p)$ is the particle position and $\tau_p = \rho_p d_p^2/18\nu\rho_f$ is the particle relaxation time. In particular, $\vec{u}_{fp} = (\tilde{u}_{fp}, \tilde{v}_{fp}, \tilde{w}_{fp})$ is the instantaneous local fluid velocity vector at the particle position in x-, y-, and z- direction, respectively. This is to be distinguished from the Eulerian fluid velocity vector at the grid points, $\vec{u}_f = (\tilde{u}_f, \tilde{v}_f, \tilde{w}_f)$. For particles, $\vec{u}_p$ is the instantaneous particle velocity vector, $\vec{u}_p = (\tilde{u}_p, \tilde{v}_p, \tilde{w}_p)$. The last term in Eq. (1b) is a semi-empirical correction for the drag force in order to extend the validity to particle Reynolds numbers $Re_p > 1$. Periodic boundary conditions were imposed in the homogeneous directions. At the no-slip walls, a perfect elastic reflection condition was applied when the distance between the particle centre and the wall is smaller than half the particle diameter d_p. We have applied the Lagrangian point-particle tracking approach in numerous studies[12,44–46] as well as in the accompanying study by Yang *et al.*[43]

Particle parameters are listed in Table II. The current study considers five groups of particles with different inertia identified by a St number, which is defined as $St = \tau_p/(\nu/u_{\tau,s}^2)$. In addition, each global St corresponds to a local Stokes number based on the local Kolmogorov microscale τ_K ($\tau_K = (\nu/\epsilon)^{1/2}$) defined as $St_K = \tau_p/\tau_K$. The relation between the global St and the local St_K would then be $St_K = St/\tau_K^+$. The local St_K can be crucial in determining particle transport.[47] Due to the

TABLE II. Particle parameters. ρ_p/ρ_f is the density ratio of particle to fluid, d_p/h is the normalized particle diameter, NP_{total} is the total number of particles in the computational domain, and St_K is the local Stokes number based on the local Kolmogorov time scale [data taken from Yang *et al.*, "Particle segregation in turbulent Couette–Poiseuille flow with vanishing wall shear," Int. J. Multiphase Flow **98**, 45–55 (2018). Copyright 2017 Elsevier B.V.].

St	ρ_p/ρ_f	$d_p/h \times 10^3$	$NP_{total} \times 10^{-6}$	St_K ($z^+ = 10$)	St_K ($z^+ = 350$)
0.2	6.94	2	2.5	0.07	0.01
1	34.72	2	2.5	0.34	0.05
5	173.6	2	2.5	1.72	0.27
30	1041.7	2	2.5	10.34	1.61
100	3472.33	2	2.5	34.46	5.36

enlargement of τ_K^+ from the stationary wall to the moving wall, St_K decreases approaching the moving wall as shown by Yang *et al.*[43] Values of St_K are given at two near-wall locations in Table II. In particular, $St = 5$ near the stationary wall and $St = 30$ near the moving wall both have St_K close to unity. This is closely associated with the particles' tendency to cluster in preferred areas.

C. A 2D Shannon entropy method

Some studies have used a one-dimensional (1D) global Shannon entropy to quantify the overall wall-normal particle segregation in wall-bounded turbulence.[24–26] With the whole computational domain divided into N_{bin} uniformly distributed wall-parallel bins, the global Shannon entropy is defined as

$$Sh(t) = H(t)/\max[H(t)] \tag{2a}$$

$$\text{with } H(t) = -\sum_{k=1}^{N_{bin}} p(k,t)\ln p(k,t) \tag{2b}$$

$$\text{and } p(k,t) = NP(k,t)/NP_{total}, \tag{2c}$$

where $p(k,t)$ is the probability of finding a particle in the kth bin at time t and $\max(H(t)) = \ln N_{bin}$. Here $NP(k,t)$ is the number of particles in the kth bin at time t and NP_{total} is the total number of particles in the whole domain. The global Shannon entropy is a box-counting method with a total of N_{bin} boxes. According to the definition [Eq. (2)], a uniformly distributed particle field results in $Sh = 1$, while the strongest wall-normal segregation (i.e., if all particles are segregated in a single bin) leads to $Sh = 0$.

Inspired by the 1D global Shannon entropy, we introduce the method of a two-dimensional (2D) Shannon entropy. In order to evaluate the pattern of 2D particle preferential concentration in the wall-parallel bins, generalized calculations are applied for box-counting in wall-parallel directions for each bin along the wall-normal direction. A sketch of the definition of the 2D Shannon entropy method is shown in Fig. 2 for a sample bin. The bin is further divided in the wall-parallel plane into n sampling cells along the streamwise direction and m sampling cells in the spanwise direction. Depending on n and m, the wall-parallel cells are coarser (e.g., when $n \times m = 5 \times 5$) or finer (e.g., when $n \times m = 100 \times 100$). In total, the cell number in the wall-parallel layer will be $n \times m$, and the box number in the whole domain will be $n \times m \times N_{bin}$. Each box is then marked by (i, j, k), where $i = 1$ to n, $j = 1$ to m, and $k = 1$ to N_{bin}. The sides of the equal-sized cells are calculated as $dx^+ = l_x^+/n$ and $dy^+ = l_y^+/m$, which therefore vary with the cell number. A 2D Shannon entropy in each wall-parallel bin k as a function of n and m can thus be defined as

$$Sh_{xy}(k,t) = H_{xy}(k,t)/\max[H_{xy}(k,t)] \tag{3a}$$

$$\text{with } H_{xy}(k,t) = -\sum_{i=1}^{n}\sum_{j=1}^{m} p(i,j,k,t)\ln p(i,j,k,t) \tag{3b}$$

$$\text{and } p(i,j,k,t) = NP(i,j,k,t)/NP(k,t), \tag{3c}$$

where $p(i, j, k, t)$ is the possibility of finding a particle in the (i,j)th cell in this sample kth bin and $\max[H_{xy}(k,t)] = \ln(n \times m)$ for each kth bin. As defined before, $NP(k,t)$ is the total number of particles in the kth bin, and $NP(i, j, k, t)$ is the number of particles in the (i,j)th cell in this bin.

The global (1D) Shannon entropy defined in Eq. (2) is used as an indicator of the degree of particle segregation in the inhomogeneous wall-normal direction in channel flow situations.[24–26] The novel 2D Shannon entropy introduced in Eq. (3) is aimed as an indicator of the degree of preferential particle concentration in wall-parallel planes and, moreover, as a means to distinguish between isotropic and anisotropic particle clustering. The 2D Shannon entropy method will be applied herein to the particulate CP flow using $N_{bin} = 360$ bins of uniform thickness $dz^+ = 1$ and cell numbers n and m both varying from 5 to 100 (i.e., n or $m = 5, 6, 7, \ldots, 100$). Correspondingly, the cell sizes $dx^+ = 129.6$–2592 and $dy^+ = 36$–720.

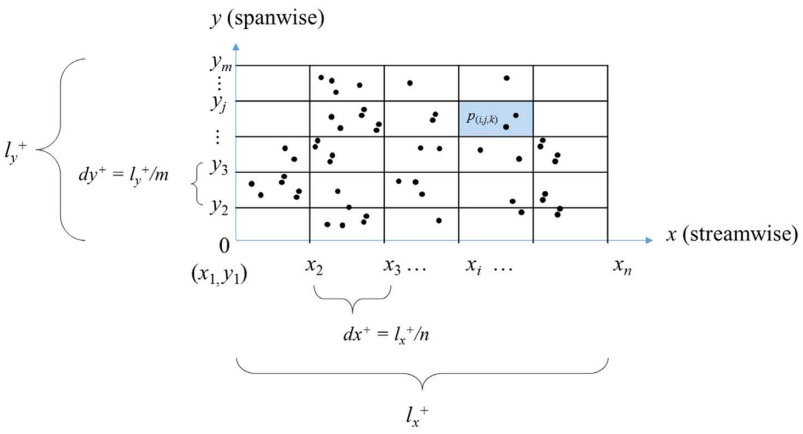

FIG. 2. Definition sketch for the 2D Shannon entropy method considering the kth bin (k = 1–360). The bin is further divided into $n \times m$ cells in the $x \times y$ directions, where n and m are the total number of cells in each direction and $n \times m$ vary from 25 ($n \times m = 5 \times 5$) to 10 000 ($n \times m = 100 \times 100$), and i and j are the indices to each individual cell. Globally, each box is then marked by (i, j, k). Note that the sizes dx and dy of the sampling cells in the wall-parallel bins should be distinguished from the sizes Δx and Δy of the computational grid used for DNS.

III. RESULTS

It has been extensively documented that inertial particles in turbulent wall-bounded flows are likely to accumulate in the near-wall region and abandon the channel centre due to turbophoresis.[11–14,25] In our current CP flow, the asymmetric wall conditions result in distinct near-wall particle segregations, depending on particle inertia.[43] Near the stationary wall, the particle segregation followed a non-monotonic trend with strongest segregation for intermediate Stokes numbers $St \approx 30$, just as repeatedly reported from P flow simulations.[11,12] The particle segregation near the moving wall, on the other hand, increased monotonically with St, as shown in Fig. 9(a) by Yang *et al.*,[43] in which a relatively wide core region with uniform but St-dependent particle concentrations was observed.

A. Characteristics of wall-parallel preferential concentration

The asymmetric flow field with respect to the centre plane will not only result in an asymmetric wall-normal segregation but also in distinctly different wall-parallel preferential concentrations, which also vary with particle inertia. Figure 3 compares the background flow field with the instantaneous particle distributions at three selected wall-parallel bins for different inertia (St = 1, 30, and 100). The sampling wall-parallel bins were chosen at the channel centre, and two near-wall

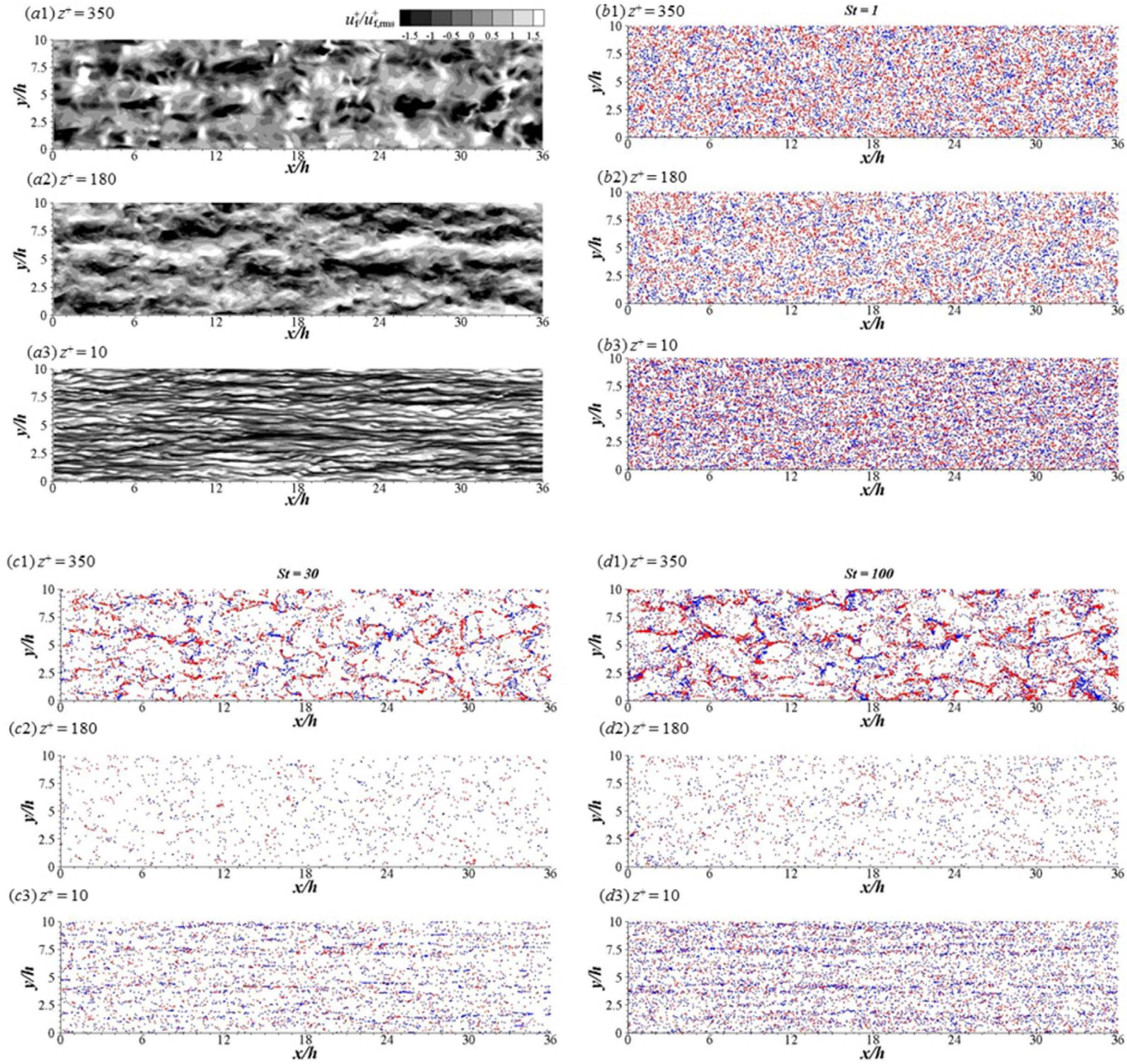

FIG. 3. Instantaneous streamwise velocity fluctuations ($|u_f^+/u_{f,rms}^+| < 1.5$) in wall-parallel planes [(a1)–(a3)] and distribution of particles with varying inertia at corresponding wall-normal locations. [(b1)–(b3)] St = 1; [(c1)–(c3)] St = 30: [(d1)–(d3)] St = 100. z^+ = 350: near the moving wall, z^+ = 180: at channel center, z^+ = 10: near the stationary wall. Colors in (b)–(d) show positive (blue) and negative (red) wall-normal particle velocities w_p.

ones symmetrically located with respect to the centre, each at an off-wall distance of 10 wall units (where the quasi-coherent turbulent structures are prominent near the stationary wall[23]). At large inertia, the wall-normal distribution of particles becomes inhomogeneous and anisotropic, with the actual distribution pattern depending on the wall-normal location. For such heavy particles, a correlation of the concentration patterns with the underlying flow structures is clearly observed. Heavy particles near the stationary wall form longitudinal streaks as they accumulate below the streamwise low-speed streaks due to the effects of the quasi-streamwise vortices flanking these streaks, similarly as in a P flow.[2,11,19] In the core region, the flow field demonstrates streamwise-oriented structures of the LSSs.[22,23,42] However, as a result of the relatively low particle population, as well as the absence of the strong near-wall turbulent structures in the channel centre, the particles exhibit an almost isotropic distribution similar to that observed in HIT, without forming any large-scale clusters with directional preference. Near the moving wall, the LSSs oriented in the streamwise direction can still be weakly recognized in the flow field [Fig. 3(a1)], although much weaker than in the centre.[23] Correspondingly, a large number of segregated particles accumulate to form filaments with a slight streamwise-orientation, demonstrating the influence of the LSSs.

To measure the inhomogeneity of the particle preferential concentration observed in Fig. 3, Fig. 4 shows the variance of Voronoï volumes near the two walls for different St values. The variance is defined as $\sigma_V^2 = \overline{(V - V_m)^2}$ for each wall-parallel kth bin, where V is the Voronoï volume for each particle and V_m is the local mean Voronoï volume in this bin. The Voronoï volumes were calculated using the same method as that described and validated by Nilsen *et al.*[6] For randomly distributed particles $\sigma_V^2/V_m^2 \approx 0.18$, and larger σ_V^2 indicates stronger inhomogeneity of the preferential concentration. As shown in Fig. 4, the St-dependence of the normalized σ_V^2 is clearly non-monotonic, with $St = 30$ having the strongest inhomogeneous particle clustering and $St = 0.2$ the weakest near both walls. Near the stationary wall, $St = 5$ and $St = 100$ particles exhibit a similar degree of inhomogeneity, but near the moving wall $St = 100$ is clearly more clustered than $St = 5$.

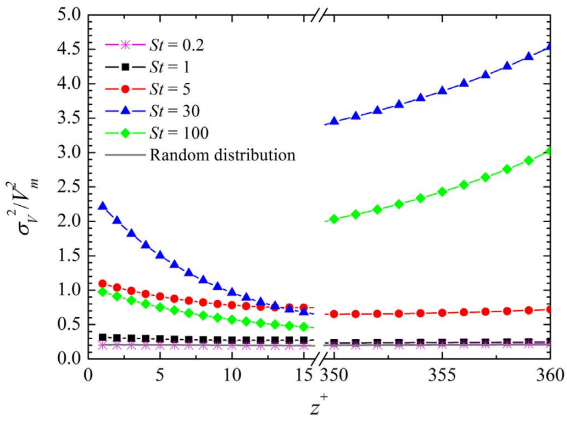

FIG. 4. Normalized variance σ_V^2/V_m^2 of the Voronoï volume for particles at different St values. Results are shown for the stationary wall region ($z^+ \le 15$) and the moving wall region ($z^+ \ge 350$). The grey line is for randomly distributed particles ($\sigma_V^2/V_m^2 \approx 0.18$).

The cluster patterns observed in Fig. 3 have qualitatively different appearances at the moving and stationary walls. These patterns are important features of the preferential concentration and reflect the anisotropy of the particle clustering. The dependence of the patterns on the wall-normal location will now be examined by means of the new 2D Shannon entropy method introduced in Sec. II C. Similarly as for the global Shannon entropy Sh defined in Eq. (2), the local Shannon entropy Sh_{xy} defined in Eq. (3) also approaches unity if the particles are equally distributed between the $n \times m$ sampling cells in a given wall-parallel bin. Therefore, as the cell sizes dy^+ and dx^+ become larger than the characteristic length scale of the clustering, Sh_{xy} approaches 1. If either dy^+ or dx^+ or both is gradually reduced, the local Shannon entropy Sh_{xy} starts to diminish when dy^+ or dx^+ becomes comparable with the size of the clusters or void areas. The local Shannon entropy is therefore a means to estimate the characteristic length scale of clustering patterns and, moreover, whether or not the length scale is the same (isotropy) or different (anisotropy) in the x- and y-direction. In Fig. 5, local Shannon entropies are shown for $St = 30$ particles, i.e., corresponding to the plots in Fig. 3(c). We immediately observe that $Sh_{xy} \approx 1$ (i.e., red) for the largest cell sizes, i.e., dx^+ or dy^+ equals the domain size ($dx^+ = 2592$ in streamwise or $dy^+ = 720$ in spanwise). These cell sizes are too long or wide for the chosen grid to resolve the clustering pattern. Here (almost) isotropy is detected in the

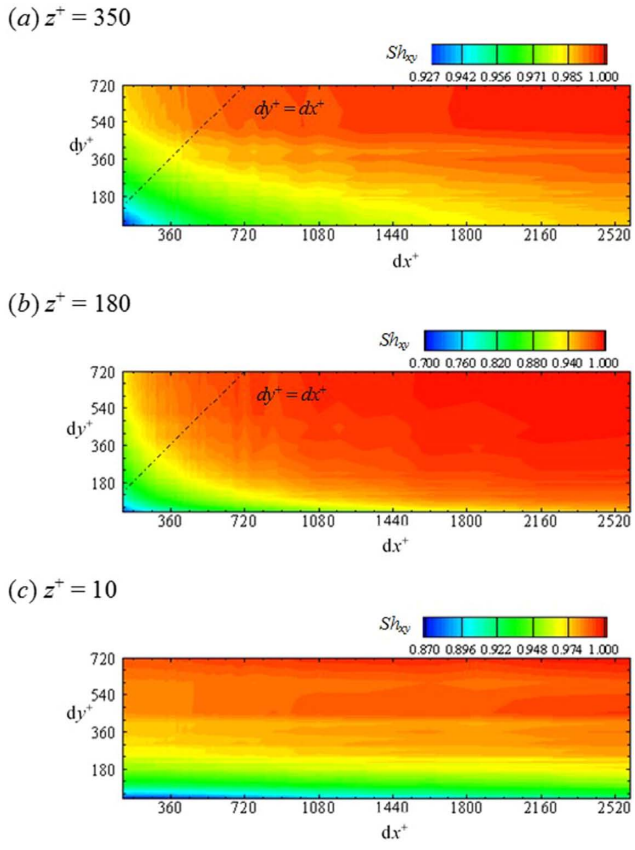

FIG. 5. Contours of Sh_{xy} calculated with different cell sizes for instantaneous particle distribution at $St = 30$ on selected wall-normal locations [corresponding to Fig. 3(c)]. Note that the horizontal axis for dx^+ starts from 129.6 and the vertical axis for dy^+ starts from 36. To facilitate our discussion, a diagonal reference line $dy^+ = dx^+$ is given by the dashed-dotted line in (a) and (b).

channel centre [Fig. 5(b)] by the symmetric contours of Sh_{xy} with respect to the reference line $dy^+ = dx^+$. The isotropy is consistent with the observation from Fig. 3. In addition, both streamwise-oriented slender cells ($dx^+ > dy^+$) and spanwise-oriented slender cells ($dx^+ < dy^+$) lead to a slightly lower Sh_{xy} than that obtained from square cells ($dx^+ = dy^+$). This indicates that the particles accumulate in filaments and leave broad areas as voids.

Breakdown of the isotropic concentration near the stationary wall is detected and the streamwise particle streaks close to the stationary wall are captured by strong dependency of the Sh_{xy} contours on dy^+ and almost independency on dx^+ (i.e., the change of dx^+ plays a much less role than the change of dy^+) in Fig. 5(c), compared to Figs. 5(a) and 5(b). The strong dy^+-dependency indicates that the degree of non-uniformity of particle distribution in the spanwise (y-) direction is much stronger than in the streamwise (x-) direction, confirming the particle preferential concentration in streamwise-oriented streaks. A closer examination of Fig. 5(c) reveals that effects of the streamwise cell size (dx^+) come into play only for $dy^+ \lesssim 100$. The critical value of $dy^+ \approx 100$ indicates an estimate of the average spanwise spacing of the particle streaks, which agrees with alternative measures in previous studies.[10,20]

The strong dy^+-dependency of Sh_{xy} disappears away from the stationary wall. The Sh_{xy} contours in the moving-wall region [Fig. 5(a)] are similar to those in the core region. The particle filaments and voids are also reflected by the fact that slender cells result in a lower Sh_{xy} than square cells. However, unlike the core region, Fig. 5(a) shows an obvious inclination towards a dy^+-dependency, indicating that the particle filaments are more often oriented in the streamwise direction, thereby confirming the observation in Fig. 3. The slight streamwise preferential concentration, which is successfully detected by the new 2D Shannon entropy method, is associated with the LSSs. Compared with near the stationary wall [Fig. 5(c)], the streamwise preference demonstrated near the moving wall [Fig. 5(a)] is substantially reduced, due to the fact that the global LSSs are much weaker in strength than the quasi-coherent turbulent structures localized near the stationary wall.

B. Mechanisms of wall-parallel preferential concentration

The wall-parallel preferential concentration described above results from several coexisting mechanisms in the present CP flow, including the strain-vorticity-selection mechanism, the quasi-coherent turbulent structures exclusively near the stationary wall, and the global LSSs. We proceed to show in this sub-section that the strain-vorticity-selection mechanism leads to an inhomogeneous particle distribution, while the coherent structures cause anisotropy of the preferential concentration. The relative importance of these mechanisms depends on the actual wall-normal location, as shown in Fig. 5. Near the stationary wall, the particle concentration is dominated by the effects of the strong quasi-coherent near-wall turbulent structures. The strain-vorticity-selection mechanism and the LSSs are most effective away from the stationary wall. We will now examine the region near the moving wall, where the particle number is sufficiently high due to segregation to demonstrate a clear preferential concentration, which reflects the combined effects of the strain-vorticity-selection and the LSSs.

First, the strain-vorticity-selection mechanism near the moving wall is considered. Inertial particles are known to gather in strain-dominating regions and to avoid vorticity-dominating regions in HIT,[2,3] due to centrifugal forces. To examine the conventional centrifugal effects on preferential concentration, Fig. 6 compares the particle preferential concentration at different St with the underlying flow field shown by velocity vectors. Wall-normal vortices of the local fluid are reflected by the vector plots. Vortex centers are where the vectors are spreading and pointing outwards, and vortex edges are where vectors meet. The particles are color-coded to show the direction and size-scaled to show the magnitude of the wall-normal particle velocity w_p^+. The wall-ward (blue) particles, since they come from the core region with relatively high turbulent intensities, obviously have larger w_p^+ than the off-wall (red) particles. With the increase of St, a general observation is a stronger trend of the particles to accumulate in the periphery of the large vortices to form filaments and to leave the vortex centres to form voids [see e.g., $St = 30$ in Fig. 6(c)]. However, for the largest Stokes number $St = 100$, many particles have large w_p^+ (either towards or away from the wall) in the near-wall region. Therefore such particles are able to

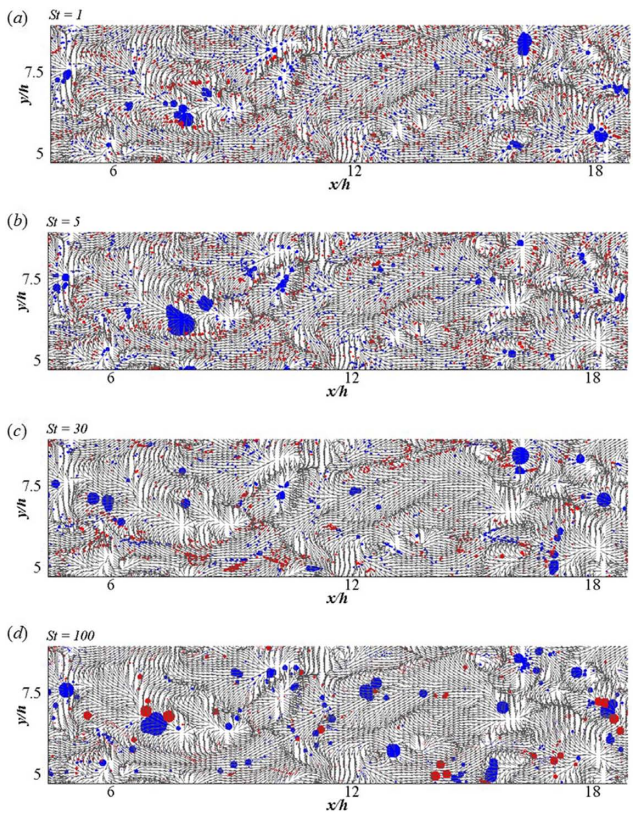

FIG. 6. Instantaneous particle distributions and fluctuating flow fields shown by fluid velocity vectors at $z^+ = 350$ near the moving wall, showing only part of the xy-domain. The background flow is the same, while the particles are of different inertia: (a) $St = 1$, (b) $St = 5$, (c) $St = 30$, and (d) $St = 100$. Particle color shows the direction of the wall-normal particle velocity w_p^+, i.e., positive or towards the wall (blue) and negative or away from the wall (red), and the particle size shows the magnitude of w_p^+.

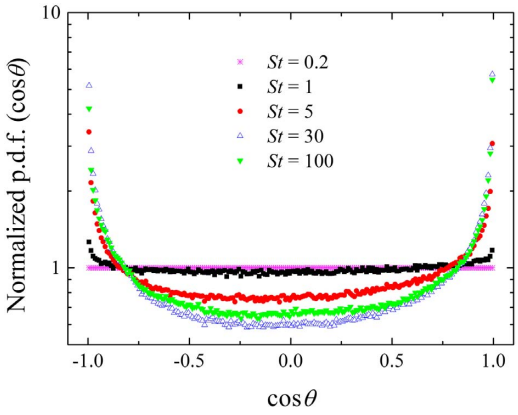

FIG. 7. Instantaneous normalized p.d.f. of $\cos\theta$ for all particle groups near the moving wall. Normalization was performed using p.d.f. ($\cos\theta$) obtained for randomly distributed particles.

overcome the local centrifugal forces and appear more often in vorticity-dominating regions, as observed in Fig. 6(d).

A quantitative representation of the strain-vorticity-selection mechanism suggested by Fig. 6 is obtained by evaluating the p.d.f. of the cosine of the angle θ between the instantaneous local fluid velocity vector ($\vec{u}_{fp}$) and the local fluid acceleration vector ($\vec{a}_{fp}$),

$$\cos\theta = \frac{\vec{u}_{fp}\cdot\vec{a}_{fp}}{\left|\vec{u}_{fp}\right|\left|\vec{a}_{fp}\right|}, \tag{4}$$

which is plotted in Fig. 7. According to the definition, when $|\cos\theta|$ equals to 1, the local fluid is in strain-dominating regions, while when $|\cos\theta|$ equals to 0, the local fluid is in vorticity-dominating regions.[48] Correlations between the local strain/vorticity and the particle concentration are quantitatively represented by the p.d.f. of $|\cos\theta|$. Inertia effects are clearly observed from Fig. 7. The strongest clustered case is $St = 30$ (in consistency with Fig. 4), which has the steepest curves with the highest probability density at $|\cos\theta| = 1$ and the lowest at $|\cos\theta| = 0$. This indicates that the strongest inertia selection by the local fluid occurs at $St = 30$, which results in the most unbalanced distribution of particles accumulating in strain-dominating regions and avoiding vorticity-dominating regions. Due to inertia effects, lighter particles or heavier particles than $St = 30$ have a more evenly distributed p.d.f. as a result of less clustering. This method provides a quantitative confirmation of the strain-vorticity-selection mechanism of the underlying fluid, which results in the inhomogeneity of the particle concentration in wall-parallel planes.

The non-monotonic St-dependency of the wall-parallel inhomogeneity can be explained in terms of the local Stokes number St_K based on the Kolmogorov time scale.[43] When inertia selection is performed by local strain or vorticity, such as in HIT, maximum preferential concentration is found for particles with response time close to the Kolmogorov time scale,[4] i.e., $St_K \approx 1$. This is also the case near the moving wall, where strong near-wall turbulent structures are absent and the inertia selection is dominated by the strain-vorticity-selection mechanism similarly as in HIT (the LSSs are weak here and only slightly influential). As shown in Table II, in this region (e.g., $z^+ \approx 350$), St_K for $St = 30$ is close to 1, while St_K for $St = 100$ (and 5) is somewhat larger (and smaller) than 1. Therefore the strongest wall-parallel particle concentration in this region occurs for $St = 30$, followed by $St = 100$ (and 5). The $St = 100$ particles are apparently too inertial to follow the fluid structures and are thus more randomly distributed. For $St = 5$, St_K is below 1, and the particle inertia is almost negligible so that the particles follow the flow more easily.

The particle preferential concentration near the moving wall demonstrates anisotropic patterns which result from the LSSs. To evaluate the effects of LSSs, Fig. 8 shows p.d.f. of $u^+_{fp}/u^+_{fp,rms}$, where u^+_{fp} is the normalized local fluid streamwise velocity fluctuation at particle locations and $u^+_{fp,rms}$ is the local r.m.s. of u^+_{fp} in each bin. For comparison, results for near the stationary wall are also presented, which can be used to evaluate the effects of the strong near-wall turbulent structures. The skewness and kurtosis of the p.d.f. curves are also calculated and given in Table III. Comparison between the two walls shows that inertial effects on particle wall-parallel preferential concentration are clearly more pronounced near the stationary wall. This is due to the selection effects of the strong near-wall turbulent structures in this region. Results for the stationary wall in Fig. 8(a) with the peaks located at the negative side of $u^+_{fp}/u^+_{fp,rms}$ agree well with the fact that the particles accumulate under the low-speed fluid streaks. This is also confirmed by the positive skewness (the curves right-skewed) indicating that the particles are concentrated in

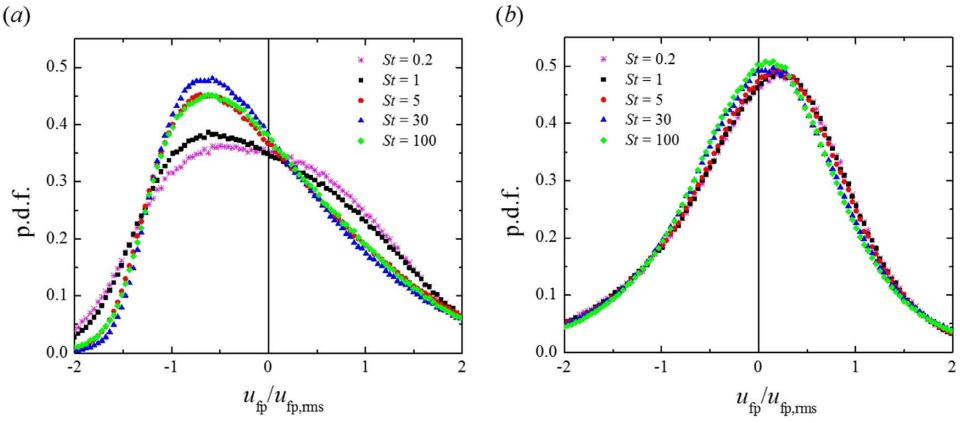

FIG. 8. P.d.f. of the normalized local fluid streamwise velocity fluctuation $u^+_{fp}/u^+_{fp,rms}$. Comparison between (a) near the stationary wall in the range of $z^+ = 1$–21 and (b) near the moving wall in the range of $z^+ = 339$–359. $u^+_{fp,rms}$ is first computed for $1\nu/u_{\tau,s}$ thick bins. The results are averaged over $20\nu/u^2_{\tau,s}$ using 58 samples.

TABLE III. Skewness and kurtosis of the p.d.f. curves of $u^+_{fp}/u^+_{fp,rms}$ plotted in Fig. 8 for different St.

	St	0.2	1	5	30	100
Skewness	Stationary wall	0.30	0.45	0.85	1.02	0.87
	Moving wall	−0.62	−0.61	−0.58	−0.39	−0.38
Kurtosis	Stationary wall	2.83	3.01	3.82	4.37	4.02
	Moving wall	4.78	4.86	5.04	5.07	5.37

areas with negative $u^+_{fp}/u^+_{fp,rms}$. Also, the largest kurtosis for $St = 30$ indicates the strongest anisotropy, i.e., the case with the highest concentration of particles in the low-speed streaks, followed by $St = 100$, 5, 1, and 0.2 in decreasing order. Near the moving wall [Fig. 8(b)], all p.d.f. curves have peaks switched to the slightly positive side of $u^+_{fp}/u^+_{fp,rms}$ (quantitatively confirmed by the negative skewness), where all particle groups are now preferentially accumulated. This observation is straightforward to interpret with observations of the background flow in Fig. 3(a1). The LSSs are oriented in the streamwise direction, and two neighbouring LSSs form a vortex pair in between where the streamwise velocity fluctuation approaches 0. Near the moving wall, particles are swept into regions between the LSSs, and those heavy particles will stay there since the local turbulent advection is too weak to re-entrain them to leave the wall region. Therefore the heavy particles will remain clustered in regions between two LSSs, where $u^+_{fp}/u^+_{fp,rms} \approx 0$, and the stronger the clustering under this $u^+_{fp}/u^+_{fp,rms}-$ region, the closer to 0 the peaks of the p.d.f. curves should be (i.e., less skewed). The two curves for $St = 30$ and 100 in Fig. 8(b) almost overlap, leading to similar skewness and kurtosis of these two cases. However, the heaviest particles of $St = 100$ have slightly smaller skewness magnitude and larger kurtosis, indicating that these particles are slightly more concentrated in regions between two LSSs. Therefore the weak St-dependency of the anisotropy near the moving wall follows a monotonically decreasing trend.

IV. CONCLUDING REMARKS

This paper focused on a numerical study of wall-parallel preferential concentration of inertial particles in a shear-free Couette-Poiseuille flow,[23] via DNS coupled with Lagrangian particle-tracing approach. The carrying flow is asymmetric with respect to the channel centre and has vanishing mean shear at the moving wall. Distinctive near-wall structures are formed in the flow, where conventional quasi-coherent turbulent streaky structures are found exclusively near the stationary wall. These streaky structures are strong and dominate the local flow field. In addition to these near-wall streaky structures, global but weak LSSs are observed in the current CP flow. These two types of coherent structures play a crucial role in wall-parallel particle concentration, and their relative effects depend on wall-normal locations.

The global Shannon entropy is an indicator of the overall degree of particle segregation but tells nothing about where and how particles are segregated. In the present study, two different approaches have been proposed to analyze particle clustering, each with its own advantages and disadvantages:

- The variance of the Voronoï volumes provides information on and also to what extent the particles are preferentially distributed in wall-parallel planes.
- The local 2D Shannon entropy is a new indicator of the degree of anisotropy of the particle clusters. The 2D Shannon entropy tells if and how the particles are preferentially concentrated in wall-parallel planes, i.e., whether the concentration is isotropic or anisotropic, and in the latter case in which direction the clusters are aligned.

An overall wall-parallel preferential concentration of heavy particles is observed to closely resemble the flow patterns and is found to be both inhomogeneous and anisotropic. The inhomogeneity refers to the particle distribution with filaments and voids due to the strain-vorticity-selection mechanism, i.e., particles' preference to accumulate in strain-dominating regions and to avoid vorticity-dominating regions. The inhomogeneity in the current CP flow similar as in HIT is quantitatively confirmed and demonstrated by p.d.f. of $\cos\theta$, where θ is the angle between the instantaneous local fluid velocity and acceleration. The strain-vorticity-selection mechanism is present in the whole domain. The overall inhomogeneity can be measured by a Voronoï method. The degree of inhomogeneity shows a non-monotonic St-dependency, where the strongest clustering is found for $St = 30$. The St-dependency of the concentration inhomogeneity is understood by evaluating the local Stokes number St_K based on the local Kolmogorov time scale. When the inertia selection is performed by a strain-vorticity-selection mechanism similar to in HIT, strongest clustering is found for $St_K \approx 1$, which is the case for $St = 30$ near the moving wall.

The anisotropy of wall-normal preferential concentration is caused by the coherent fluid structures and therefore varies from wall to wall in the asymmetric flow field. The flow near the stationary wall is dominated by the quasi-coherent turbulent structures which cause the particles to accumulate under the low-speed fluid regions and form streamwise-oriented streaks. Away from the stationary wall, the anisotropy of particle concentration results from the global LSSs. Due to wall-normal particle segregation[43] that has caused depletion of particles in the core region and segregation near the walls, the effects of LSSs on the wall-parallel concentration are not apparent in the channel centre but can be clearly observed near the moving wall. In this region, the particle preferential concentration demonstrates a pattern of slightly streamwise-oriented filaments, which results from combined effects of the strain-vorticity-selection and the LSSs. The anisotropy of particle wall-parallel preferential concentration can be detected with a new 2D Shannon entropy method, introduced in the current study for the first time. The 2D Shannon entropy is a box-counting method, and by evaluating the change of the contours of the 2D Shannon entropy following the variation of the sizes of the sampling cells, the patterns of the particle concentration can be obtained. The effects of the coherent flow structures on the particle anisotropy can be quantified by means of p.d.f. of the local fluid velocity, which reveals a

non-monotonic St-dependency of the degree of anisotropy near the stationary wall (with the most anisotropic case at $St = 30$) and a weak monotonic St-dependency near the moving wall (with the most anisotropic case at $St = 100$).

ACKNOWLEDGMENTS

The work is supported by The Research Council of Norway (NFR) under Grant No. 250744 (K.Y. and H.I.A.) and Natural Science Foundation of China through Grant Nos. 11702158 and 11490551 (L.Z.). Our thanks go to Sigma2 for their support of computational resources through Grant No. NN2649K. We would also like to express our sincere thanks to Dr. Christopher Nilsen from University of Bergen and Ms. Judith Elin Vesper (now at TU Delft) for helpful discussions on the Voronoï volume method.

[1] R. Monchaux, M. Bourgoin, and A. Cartellier, "Analyzing preferential concentration and clustering of inertial particles in turbulence," Int. J. Multiphase Flow **40**, 1–18 (2012).
[2] K. D. Squires and J. K. Eaton, "Preferential concentration of particles by turbulence," Phys. Fluids A **3**, 1169–1178 (1991).
[3] L.-P. Wang and M. R. Maxey, "Settling velocity and concentration distribution of heavy particles in homogeneous isotropic turbulence," J. Fluid Mech. **256**, 27–68 (1993).
[4] R. Monchaux, M. Bourgoin, and A. Cartellier, "Preferential concentration of heavy particles: A Voronoï analysis," Phys. Fluids **22**, 103304 (2010).
[5] S. Goto and J. C. Vassilicos, "Sweep-stick mechanism of heavy particle clustering in fluid turbulence," Phys. Rev. Lett. **100**, 054503 (2008).
[6] C. Nilsen, H. I. Andersson, and L. Zhao, "A Voronoï analysis of preferential concentration in a vertical channel flow," Phys. Fluids **25**, 115108 (2013).
[7] Y. Tagawa, J. M. Mercado, V. N. Prakash, E. Calzavarini, C. Sun, and D. Lohse, "Three-dimensional Lagrangian Voronoï analysis for clustering of particles and bubbles in turbulence," J. Fluid Mech. **693**, 201–215 (2012).
[8] A. Dejoan and R. Monchaux, "Preferential concentration and settling of heavy particles in homogeneous turbulence," Phys. Fluids **25**, 013301 (2013).
[9] M. García-Villalba, A. G. Kidanemariam, and M. Uhlmann, "DNS of vertical plane channel flow with finite-size particles: Voronoï analysis, acceleration statistics and particle-conditioned averaging," Int. J. Multiphase Flow **46**, 54–74 (2012).
[10] K. M. O. Håkansson, M. Kvick, F. Lundell, L. P. Wittberg, and L. D. Söderberg, "Measurement of width and intensity of particle streaks in turbulent flows," Exp. Fluids **54**, 1555 (2013).
[11] C. Marchioli and A. Soldati, "Mechanisms for particle transfer and segregation in a turbulent boundary layer," J. Fluid Mech. **468**, 283–315 (2002).
[12] L. Zhao, C. Marchioli, and H. I. Andersson, "Stokes number effects on particle slip velocity in wall-bounded turbulence and implications for dispersion models," Phys. Fluids **24**, 021705 (2012).
[13] M. Caporaloni, F. Tampieri, F. Trombetti, and O. Vittori, "Transfer of particles in nonisotropic air turbulence," J. Atmos. Sci. **32**, 565–568 (1975).
[14] M. Reeks, "The transport of discrete particles in inhomogeneous turbulence," J. Aerosol Sci. **14**, 729–739 (1983).
[15] J. K. Eaton and J. Fessler, "Preferential concentration of particles by turbulence," Int. J. Multiphase Flow **20**, 169–209 (1994).
[16] B. van Haarlem, B. J. Boersma, and F. T. M. Nieuwstadt, "Direct numerical simulation of particle deposition onto a free-slip and no-slip surface," Phys. Fluids **10**, 2608–2620 (1998).
[17] C. Narayanan, D. Lakehal, L. Botto, and A. Soldati, "Mechanisms of particle deposition in a fully developed turbulent open channel flow," Phys. Fluids **15**, 763–775 (2003).
[18] S. Balachandar and J. K. Eaton, "Turbulent dispersed multiphase flow," Annu. Rev. Fluid Mech. **42**, 111–133 (2010).
[19] Y. Pan and S. Banerjee, "Numerical simulation of particle interactions with wall turbulence," Phys. Fluids **8**, 2733–2755 (1996).
[20] M. Bernardini, S. Pirozzoli, and P. Orlandi, "The effect of large-scale turbulent structures on particle dispersion in wall-bounded flows," Int. J. Multiphase Flow **51**, 55–64 (2013).
[21] T. Tsukahara, H. Kawamura, and K. Shingai, "DNS of turbulent Couette flow with emphasis on the large-scale structure in the core region," J. Turbul. **7**, N19 (2006).
[22] S. Pirozzoli, M. Bernardini, and P. Orlandi, "Large-scale motions and inner/outer layer interactions in turbulent Couette–Poiseuille flows," J. Fluid Mech. **680**, 534–563 (2011).
[23] K. Yang, L. Zhao, and H. I. Andersson, "Turbulent Couette–Poiseuille flow with zero wall shear," Int. J. Heat Fluid Flow **63**, 14–27 (2017).
[24] F. Picano, G. Sardina, and C. M. Casciola, "Spatial development of particle-laden turbulent pipe flow," Phys. Fluids **21**, 093305 (2009).
[25] G. Sardina, P. Schlatter, L. Brandt, F. Picano, and C. M. Casciola, "Wall accumulation and spatial localization in particle-laden wall flows," J. Fluid Mech. **699**, 50–78 (2012).
[26] M. Bernardini, "Reynolds number scaling of inertial particle statistics in turbulent channel flows," J. Fluid Mech. **758**, R1 (2014).
[27] B. Pandey, "A method for testing the cosmic homogeneity with Shannon entropy," Mon. Not. R. Astron. Soc. **430**, 3376–3382 (2013).
[28] K. C. Kim and R. J. Adrian, "Very large-scale motion in the outer layer," Phys. Fluids **11**, 417–422 (1999).
[29] M. Bernardini, S. Pirozzoli, and P. Orlandi, "Velocity statistics in turbulent channel flow up to $Re_\tau = 4000$," J. Fluid Mech. **742**, 171–191 (2014).
[30] A. Lozano-Durán and J. Jiménez, "Effect of the computational domain on direct simulations of turbulent channels up to $Re_\tau = 4200$," Phys. Fluids **26**, 011702 (2014).
[31] M. Lee and R. D. Moser, "Direct numerical simulation of turbulent channel flow up to $Re_\tau \approx 5200$," J. Fluid Mech. **774**, 395–415 (2015).
[32] M. J. Lee and J. Kim, "The structure of turbulence in a simulated plane Couette flow," in *Proceedings of 8th Symposium on Turbulent Shear Flows, Munich, Germany*, 1991, pp. 5-3-1–5-3-6.
[33] K. H. Bech, N. Tillmark, P. H. Alfredsson, and H. I. Andersson, "An investigation of turbulent plane Couette flow at low Reynolds numbers," J. Fluid Mech. **286**, 291–325 (1995).
[34] O. Kitoh, K. Nakabyashi, and F. Nishimura, "Experimental study on mean velocity and turbulence characteristics of plane Couette flow: Low-Reynolds-number effects and large longitudinal vortical structure," J. Fluid Mech. **539**, 199–227 (2005).
[35] D. H. Richter and P. P. Sullivan, "Momentum transfer in a turbulent, particle-laden Couette flow," Phys. Fluids **25**, 053304 (2013).
[36] D. H. Richter and P. P. Sullivan, "Modification of near-wall coherent structures by inertial particles," Phys. Fluids **26**, 103304 (2014).
[37] E. M. Thurlow and J. C. Klewicki, "Experimental study of turbulent Poiseuille–Couette flow," Phys. Fluids **12**, 865–875 (2000).
[38] G. N. Coleman, S. Pirozzoli, M. Quadrio, and P. R. Spalart, "Direct numerical simulation and theory of a wall-bounded flow with zero skin friction," Flow, Turbul. Combust. (in press).
[39] K. Lam and S. Banerjee, "On the condition of streak formation in a bounded turbulent flow," Phys. Fluids A **4**, 306–320 (1992).
[40] R. Nagaosa and R. A. Handler, "Statistical analysis of coherent vortices near a free surface in a fully developed turbulence," Phys. Fluids **15**, 375–394 (2003).
[41] S. Banerjee, "Upwellings, downdrafts, and whirlpools: Dominant structures in free surface turbulence," Appl. Mech. Rev **47**, S166–S172 (1994).
[42] K. Yang, L. Zhao, and H. I. Andersson, "Scales of a turbulent Couette-Poiseuille flow with vanishing mean wall shear," in *Proceedings of 9th National Conference on Computational Mechanics (MekIT 17)* (CIMNE, 2017), pp. 441–453.
[43] K. Yang, L. Zhao, and H. I. Andersson, "Particle segregation in turbulent Couette–Poiseuille flow with vanishing wall shear," Int. J. Multiphase Flow **98**, 45–55 (2018).
[44] P. Mortensen, H. I. Andersson, J. J. J. Gillissen, and B. J. Boersma, "Dynamics of prolate ellipsoidal particles in a turbulent channel flow," Phys. Fluids **20**, 093302 (2008).
[45] L. Zhao, H. I. Andersson, and J. J. J. Gillissen, "Turbulence modulation and drag reduction by spherical particles," Phys. Fluids **22**, 081702 (2010).
[46] L. Zhao and H. I. Andersson, "On particle spin in two-way coupled turbulent channel flow simulations," Phys. Fluids **23**, 093302 (2011).
[47] F. Picano, G. Sardina, P. Gualtieri, and C. M. Casciola, "Anomalous memory effects on transport of inertial particles in turbulent jets," Phys. Fluids **22**, 051705 (2010).
[48] M. Gibert, H. Xu, and E. Bodenschatz, "Where do small, weakly inertial particles go in a turbulent flow?," J. Fluid Mech. **698**, 160–167 (2012).